CARBON-EPOXY LAMINATED CYLINDRICAL SHELLS UNDER AXIAL COMPRESSION

Chiara Bisagni

Dipartimento di Ingegneria Aerospaziale
Politecnico di Milano
Via Golgi 40, 20133 Milano, Italy
e-mail: chiara@aero.polimi.it

Abstract

This work is part of a research project aimed at improving the knowledge of the buckling phenomena of composite shells.
Experimental buckling tests are performed on laminated cylindrical shells under axial compression, by a loading rig controlled in displacement. The shells, fabricated by AGUSTA, are laminated with carbon fabric layers embedded into an epoxy resin matrix and present two different types of lay-up orientation: [0°/45°/-45°/0°] and [45°/-45°/-45°/45°].
The buckling phenomena is numerically studied, taking into account the effect of the geometric imperfections, by three finite element codes: MARC, ABAQUS and ABAQUS/EXPLICIT. Using the implicit codes, the buckling has been analysed by the eigenvalue analysis and the non-linear Riks method. The explicit code has allowed to investigate the load-displacement curve, even in the post-buckling region, simulating the dynamics of a slow compression test.
Afterwards, the first results obtained by the numerical simulation of a experimental buckling test are presented here.

List of symbol

L	cylinder's length
R	cylinder's radius
t	cylinder's thickness
w	mean cylinder surface's shift
a	imperfection's amplitude
ε	nondimensional imperfection's amplitude
z	axial coordinate
ϑ	circumferential coordinate
m	number of axial semi-waves
Λ	knock down factor

Introduction

The rotorcrafts, where the weight saving is even more important than for fixed wing aircrafts, have been among the first flying machines adopting structural components made by composite materials (Ref. 1). Some very important problems, such as fatigue in rotor blades, have been well identified and almost completely solved, while for others a solution seems not well indicated till now. This is particularly true in the case of buckling strength prediction of composite shell structures, where the initial geometric imperfections, due to the manufacture process, highly influence the buckling behaviour, producing discrepancies between the experimental results and the analytical and numerical estimates (Refs. 2 - 6).
The behaviour of carbon-epoxy laminated cylindrical shells under axial compression has been investigated in the work presented here. The investigation is performed both experimentally, by means of an ad-hoc equipment, and numerically, using implicit (MARC and ABAQUS) and explicit (ABAQUS/EXPLICIT) finite element codes, and taking into account the effect of the geometric imperfections on the buckling loads.
The experimental tests have been numerically simulated using the geometric imperfections measured on the real specimens and with due considerations to the stiffness of the clamping system.
These finite element models, validated by the experimental tests (Refs. 7, 8), are began to be used to perform a sensitivity analysis. In particular the influence on the buckling load of the initial imperfections and of other geometric parameters like the thickness and the layers position has been studied.
It can contribute to a better definition of applicable strength design criteria for composite shells in buckling and post-buckling, with the final aim of a larger structure weight saving.

Cylindrical shells

The examined specimens (Figure 1) are fabricated by AGUSTA S.p.A and are characterised by the geometric properties reported in Table 1.

Table 1 - Geometric properties of the specimens

Length L *[mm]*	700
Radius R *[mm]*	350
Thickness t *[mm]*	1.32

They present two thicker reinforced ends at the top and bottom to facilitate the fixing into the loading rig. The actual specimen length is therefore limited to the central part of the cylinder and is equal to 540 *mm*.

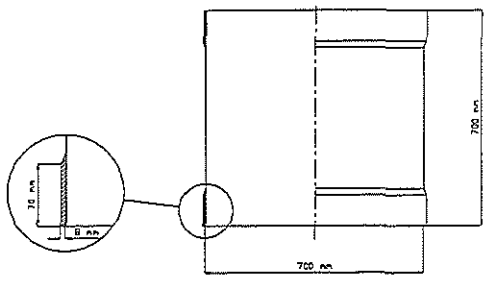

Figure 1 - Cylindrical specimen

The shells are laminated with carbon fabric layers embedded into an epoxy resin matrix. The layer properties are reported in Table 2, where x_1 and x_2 are the orthogonal in-plane axes.

Table 2 - Properties of the specimens layers

E_{11} E_{22} *[N/mm²]*	52000
G_{12} G_{13} G_{23} *[N/mm²]*	2350
ν_{12}	0.302

The specimens present two different types of lay-up orientations: [0°/45°/-45°/0°] and [45°/-45°/-45°/45°].

Experimental buckling tests

The experimental buckling tests are performed on the laminated cylindrical shells under axial compression, by a loading rig controlled in displacement (Figure 2).
A hydraulic ram generates the axial load applied on four ball screws, which in turn distribute the real applied load on the specimen. The screws are placed on the four corners of the loading platform and are driven by four stepping motors, through four reduction gears. The loading platform is software controlled giving exactly the desidered displacement. Thus the load's level, which is transferred gradually to the cylinder, depends only on the platform's displacement and by the cylinder's elastic response. It does not substantially depend on the load's magnitude that the hydraulic ram exerts on the platform.
The compression load and the axial displacement respectively are measured during the tests by three load cells, located under the lower clamp, and by three LVDT transducers, which measure the distance between the two clamps.

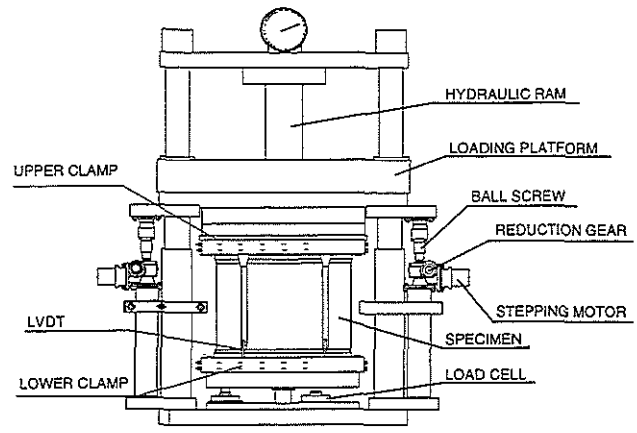

Figure 2 - Equipment for the buckling tests

An ad-hoc equipment (Ref. 9, 10) allows the measurements of geometric imperfections and buckling pattern development on the specimen's internal surface.
These measurements are obtained by five laser displacement sensors, fixed on a slide, capable of rotating and vertically translating. These movements are generated by two stepping motors. The measurements are limited to the cylinder's central part, over a length of 450 *mm*.
The vertical position of the slide is determined by an incremental encoder. The laser displacement sensors are placed at the distance of 40 *mm* from the specimen's internal surface. They guarantee a measurement range of ±10 *mm* with a resolution of 15 μ*m*, for recording of both the geometric imperfections (some tens of micrometers) and the buckling pattern (about 10 - 20 *mm*).
The equipment allows the recording of geometric imperfections and of buckling pattern on the cylinder's internal surface before the test and about 15-20 times during the tests itself; in fact the time required to measure a complete surface is limited to 4 minutes. The measurements are recorded in a regular mesh of points 10 *mm* spaced both circumferentially and axially.
Figure 3 and 4 show two typical histories of the compression load versus the axial displacement for two cylinders with [0°/45°/-45°/0°] and [45°/-45°/-45°/45°] orientation respectively. Both loading and unloading sequences are reported.
A typical buckling pattern for a cylinder with the [0°/45°/-45°/0°] lay-up orientation is reported in Figure 5. It shows 9 circumferential waves and 2 axial waves. At the recorded maximum axial displacement in the post-buckling region, the displacements normal to the surface reach 12 *mm* internally and 6 *mm* externally.

Figure 6 shows a typical buckling pattern for a cylinder with the [45°/-45°/-45°/45°] lay-up orientation. In this case 7 circumferential and 1 axial waves appear and the displacements reach 16 and 6 *mm* internally and externally respectively.

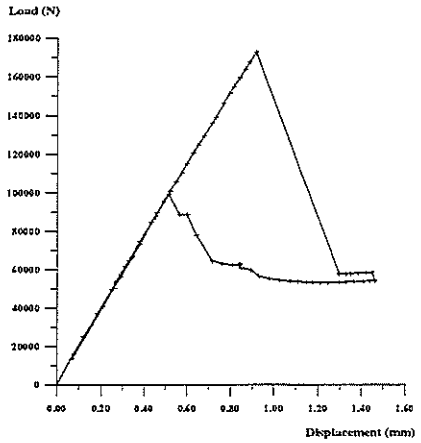

Figure 3 - Compression load versus axial displacement: cylinder [0°/45°/-45°/0]

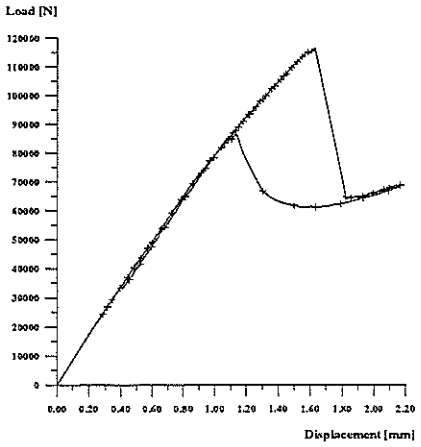

Figure 4 - Compression load versus axial displacement: cylinder [45°/-45°/-45°/45°]

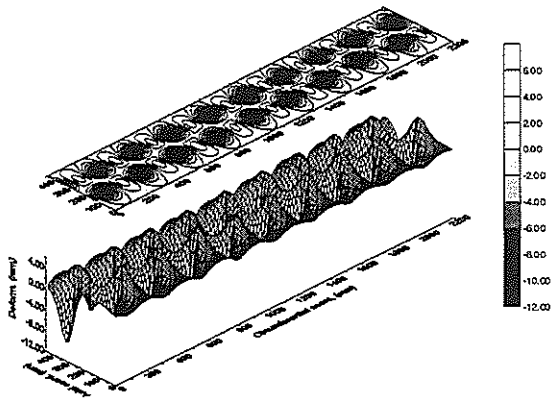

Figure 5 - Typical buckling pattern for a cylinder [0°/45°/-45°/0°]

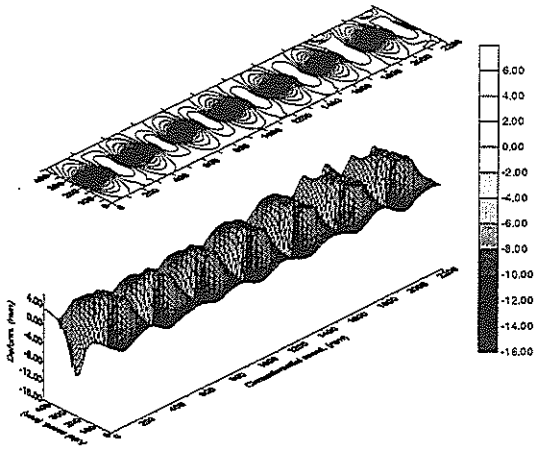

Figure 6 - Typical buckling pattern for a cylinder [45°/-45°/-45°/45°]

Finite element analysis

The experimental investigation is supported by a finite element analysis (Ref. 11), aiming at the set-up of numerical models, having the same characteristics as the real specimens and being able to reproduce the results of the experimental tests, i.e. both the buckling load values and the post-buckling behaviour. These validated models could be useful in understanding the conditions that mainly influence the buckling phenomena and in performing a wide sensitivity study, fundamental to the definition of strength design criteria.

The finite element codes used are MARC, ABAQUS and ABAQUS/EXPLICIT. In the case of the implicit codes, the buckling is analysed by the eigenvalue and the non-linear Riks methods (Ref. 12). The explicit code allows for the investigation of the load-displacement curve, even in the post-buckling region, simulating the dynamics of a slow compression test.

MARC (version K6.1) is implemented on a Hewlett Packard HP712/60 workstation, while ABAQUS (version 5.4) and ABAQUS/EXPLICIT (version 5.5) are implemented on a multiprocessor Convex Exemplar.

Implicit codes

At first, a buckling eigenvalue analysis is performed using two implicit codes: MARC and ABAQUS.

The cylinders are considered without initial imperfections, for comparison of the numerical results to the analytical predictions.

Because of the two thicker reinforced ends at the top and bottom of the cylindrical shells, the finite element model's length is taken to be 560 *mm*. This value is equal to the length of the specimen's central part, 540 *mm*, plus 10 *mm* for each part. The other geometric dimensions and the material properties are the same as for the real shells.

The upper and lower ends of the considered cylinders are supposed to remain plane and circular, maintaining the initial radius. The cylinders are modelled using 4-node bilinear shell elements (MARC element 75 and ABAQUS element S4R5).
Different meshes, modelled by 55-66-90-110-165-220 circumferential and 14-18-24-28-42-56 axial elements respectively, have been analysed. The elements dimensions are then in the different cases 40x40 *mm*, 33.33x31.11 *mm*, 24.44x23.33 *mm*, 20x20 *mm*, 13.33x13.33 *mm* and 10x10 *mm*. Using the code MARC, the two finer meshes have not been considered because of computer hardware limitations.
Tables 3 and 4 summarise the errors of the buckling loads calculated numerically against the analytical predictions (Ref. 13), for the two layers orientations and the two implicit codes.
The same results are graphically reported in Figure 7 in a logarithmic scale.

Table 3 - Errors with respect to the analytical solution: cylinder [0°/45°/-45°/0°]

	Error *[%]* MARC	Error *[%]* ABAQUS
Mesh 55 x 14	58.3	26.4
Mesh 66 x 18	40.0	20.3
Mesh 90 x 24	20.9	16.8
Mesh 110 x 28	14.0	11.3
Mesh 165 x 42	//	6.6
Mesh 220 x 56	//	3.3

Table 4 - Errors with respect to the analytical solution: cylinder [45°/-45°/-45°/45°]

	Error *[%]* MARC	Error *[%]* ABAQUS
Mesh 55 x 14	110.1	8.9
Mesh 66 x 18	69.8	4.8
Mesh 90 x 24	39.1	2.7
Mesh 110 x 28	29.5	2.2
Mesh 165 x 42	//	1.3
Mesh 220 x 56	//	1.0

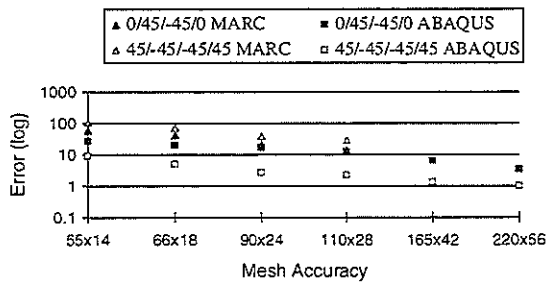

Figure 7 - Errors with respect to the analytical solutions

By increasing the mesh's accuracy, the buckling load goes towards the analytical value, resulting in errors of about 1-3% for the finest meshes (220 x 56 elements).
Buckling load variation law changes for different codes and for different orientations. The two codes yield about the same results for the cylinders with the orientation [0°/45°/-45°/0°], while for the cylinders with orientations [45°/-45°/-45°/45°] bigger differences are present. The convergence to the analytical value is quicker for ABAQUS than for MARC. Even if the results for the finer meshes are not available for the code MARC because of computer limitations, it may be extrapolated that the final MARC results will not have error of the same order of magnitude as the ABAQUS fine mesh results.
The buckling pattern for the cylinders without geometric imperfections depends on the lay-up orientations. The cylinder with orientation [0°/45°/-45°/0°] exhibits an asymmetric mode with 14 circumferential waves and 7 axial waves [Figure 8], while the cylinder with the orientation [45°/-45°/-45°/45°] exhibits an axisymmetric mode with 11 axial semi-waves [Figure 9].

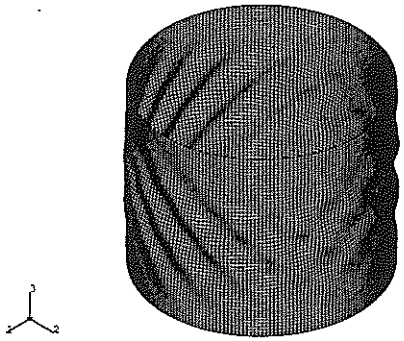

Figure 8 - Numerical buckling pattern for a cylinder [0°/45°/-45°/0°]

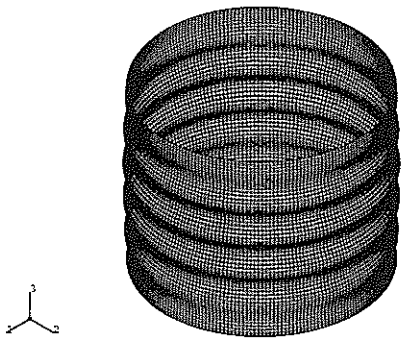

Figure 9 - Numerical buckling pattern for a cylinder [45°/-45°/-45°/45°]

Using the implicit codes, the buckling has also been analysed by the non-linear Riks method to further support the experimental study. The values of the

buckling loads obtained by the Riks method with a mesh of 110 x 28 elements are reported in the Table 5, where they are compared to the analytical values and the numerical ones obtained by the eigenvalue analysis.

Table 5 - Comparison between linear and non-linear buckling loads

	Cylinder [0°/45°/-45°/0°]	Cylinder [45°/-45°]s
Analytical sol.	240000	118580
Eigenvalue anal. MARC	273500	153566
Eigenvalue anal. ABAQUS	268430	121150
Non linear anal. MARC	268514	142600
Non linear anal. ABAQUS	266300	120230

Explicit code

The explicit code ABAQUS/EXPLICIT has allowed for the investigation of the load-displacement curve, even in the post-buckling region, simulating the dynamics of a slow compression test with an imposed displacement.
At first, the two cylinders with the two different orientations have been analysed without initial imperfections. The values of the buckling loads obtained with a mesh of 110x28 elements are compared to the analytical ones and to the results of the numerical analysis produced by the implicit codes in Table 6.

Table 6 - Comparison between buckling loads calculated by implicit and explicit codes

	Cylinder [0°/45°/-45°/0°]	Cylinder [45°/-45°]s
Analytical sol.	240000	118580
Implicit code MARC	268514	142600
Implicit code ABAQUS	266300	120230
Explicit code ABAQUS/ EXPLICIT	256920	121830

The explicit code is able to follow the curve of the axial reaction force versus the imposed displacement even in the post-buckling region. On the contrary, because of the great instabilities in the numerical solution, the analysis based on the Riks method using the implicit codes stops shortly after the maximum point of the curve, which defines the buckling load.
The load-displacement curves obtained by the code ABAQUS/EXPLICIT and by the code MARC are given for the two considered lay-up orientations in Figures 10 and 11.

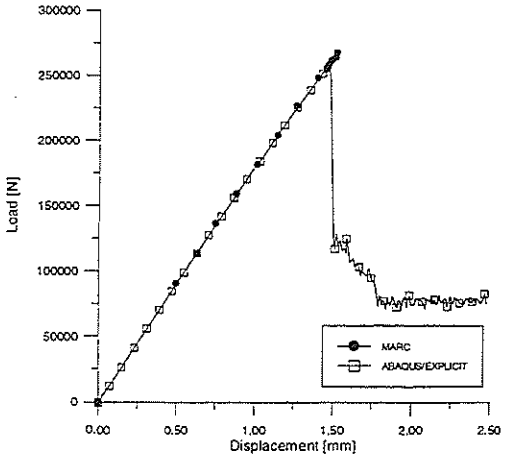

Figure 10 - Load-displacement curves : cylinder [0°/45°/-45°/0°]

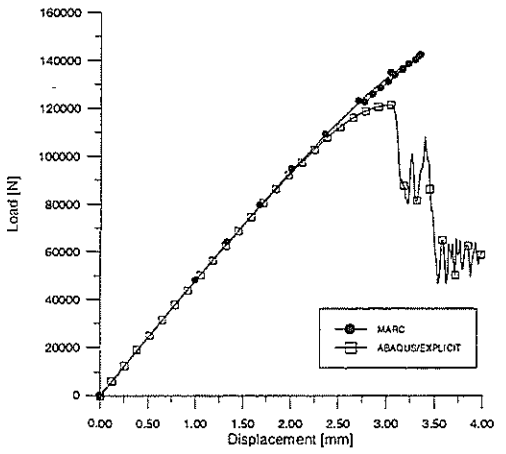

Figure 11 - Load-displacement curves: cylinder [45°/-45°/-45°/45°]

Effect of the imperfection's amplitude

Geometric imperfections are introduced into the models to study their effect on the buckling load for different amplitudes. As a consequence of the manufacturing process of the composite shells, many types of imperfections such as thickness variations and local delaminations can appear in the real specimens. In particular, many papers can be found in the literature, concerning the buckling load sensitivity with respect to the thickness variations.
The main purpose of the present work is to investigate the influence of the local variation in the cylinder's diameter on the buckling load, i.e. a shift in the mean surface of the imperfect cylinder from that of a perfect one, due, for example, to an incorrect lamination.

Axisymmetric imperfections are studied here. Namely the imperfections that present a shape similar to the buckling mode of the perfect cylinder are considered, because they are the most critical in accordance with Koiter's imperfection sensitivity theory.
The analysis is done with the implicit code MARC and the explicit code ABAQUS/EXPLICIT using a mesh of 110x28 elements. The analytical expression used to define the axisymmetric geometric imperfection is:

$$w(z,\vartheta) = a \sin(m\pi z/L)$$

where:

z = axial coordinate
ϑ = circumferential coordinate
m = number of axial semi-waves
a = imperfection's amplitude
L = cylinder's length

Because the influence of the geometric imperfections depends on the imperfection's amplitude, the analysis has been performed using eight different values for the nondimensional imperfection's amplitude ε, here defined as:

$$\varepsilon = a/t$$

($t = 1.32$ *mm*) assuming the following values:
ε = 0 - 0.01 - 0.05 - 0.125 - 0.25 - 0.50 - 0.75 - 1.00

For the cylinder with the orientation [0°/45°/-45°/0°], an imperfection of 12 axial semi-waves is used, while in the model of the cylinder with the orientation [45°/-45°/-45°/45°], an imperfection of 11 axial semi-waves is introduced.
Tables 7 and 8 report the ratio between the buckling loads obtained using the two codes for the imperfect cylinders and those of the corresponding cylinders without imperfections for the two considered orientations respectively. This ratio is called the *knock-down factor* (defined here as Λ) and it is an index of the sensitivity of the buckling load with respect to the considered geometric imperfections. The same results are graphically presented in Figures 12 and 13, where the knock-down factors versus the imperfection's amplitude are reported.

Table 7 - Knock-down factors: cylinder [0°/45°/-45°/0°]

ε	Λ MARC	Λ ABAQUS/ EXPLICIT
.000	1.000	1.000
.010	0.950	0.978
.050	0.751	0.855
.125	0.645	0.687
.250	0.512	0.535
.500	0.311	0.374
.750	0.253	0.293
1.00	0.220	0.243

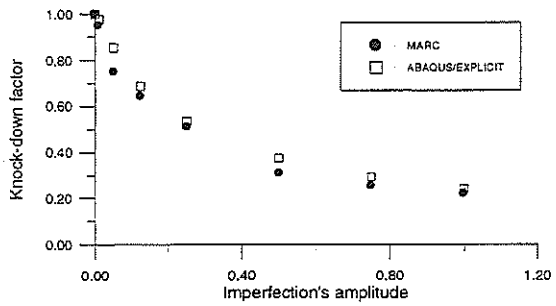

Figure 12 - Knock-down factors versus imperfection's amplitude: cylinder [0°/45°/-45°/0°]

Table 8 - Knock-down factors: cylinder [45°/-45°/-45°/45°]

ε	Λ MARC	Λ ABAQUS/ EXPLICIT
.000	1.000	1.000
.010	0.995	0.995
.050	0.959	0.955
.125	0.883	0.877
.250	0.751	0.761
.500	0.518	0.619
.750	0.476	0.515
1.00	0.394	0.447

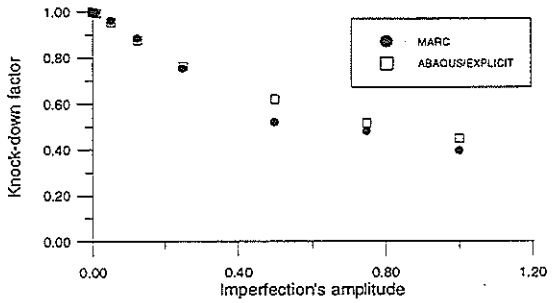

Figure 13 - Knock-down factors versus imperfection's amplitude: cylinder [45°/-45°/-45°/45°]

From the two graphs of the knock-down factor (Figures 12 and 13) it is possible to see the high sensitivity of the cylindrical shell buckling load to the geometric imperfections.
For the cylinder with [0°/45°/-45°/0°] lay-up orientation and an imperfection amplitude equal to 25% of the thickness, the buckling load is almost the half of the buckling load for a cylinder without imperfections, while for amplitude equal to the thickness, it is a quarter of the original one.
The cylinder with [45°/-45°/-45°/45°] lay-up orientation appears as less sensitive to the geometric imperfections. For an amplitude corresponding to 25% of the cylinder thickness, the buckling load is about the 75% of the

buckling load for a cylinder without imperfections, while for amplitude equal to the thickness it is about the 40%.
The resulting curves indicate that with an increase in the imperfection's amplitude, the buckling loads decrease, with this decrease being biggest for small amplitude imperfections.
Figures 14-17 show, respectively, the equilibrium curves of the compression loads versus the axial displacement for the cylinder with [0°/45°/-45°/0°] lay-up orientation and for the cylinder with [45°/-45°/-45°/45°] lay-up orientation obtained with MARC and ABAQUS/EXPLICIT.
It can be seen that for imperfection amplitude values greater than 50% of the cylinder thickness, in the post-buckling phase, the curve continues to increase with displacement but with a slope significantly smaller than in the pre-buckling phase.
The results obtained with the two codes, one implicit and the other explicit, are in agreement.

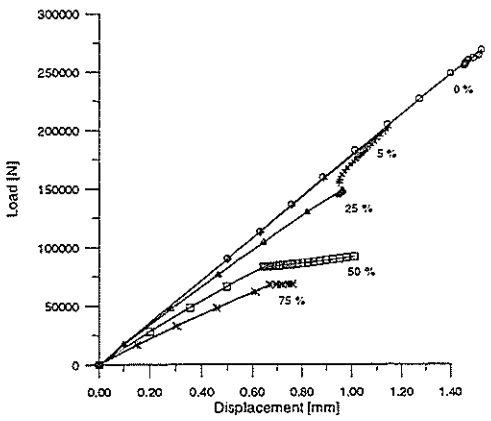

Figure 14 - Load-displacement curve:
code MARC
cylinder [0°/45°/-45°/0°]

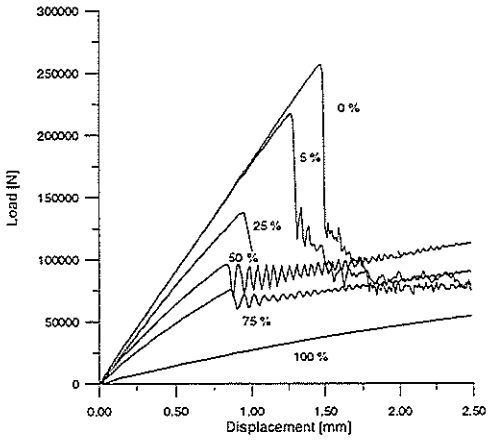

Figure 15 - Load-displacement curve:
code ABAQUS/EXPLICIT
cylinder [0°/45°/-45°/0°]

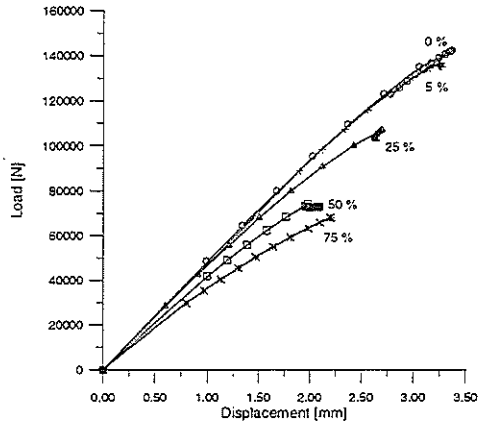

Figure 16 - Load-displacement curve:
code MARC
cylinder [45°/-45°/-45°/45°]

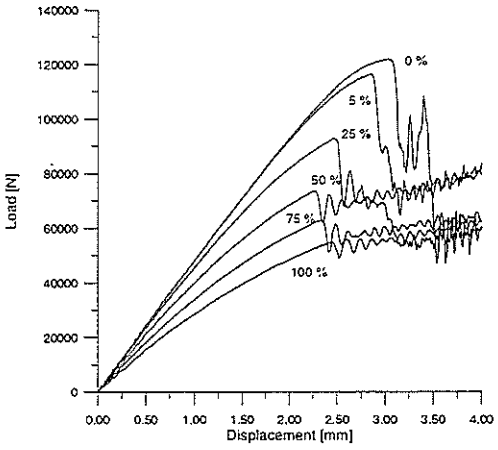

Figure 17 - Load-displacement curve:
code ABAQUS/EXPLICIT
cylinder [45°/-45°/-45°/45°]

Simulation of the experimental tests

The simulation of the experimental tests has been performed with both, the two implicit codes MARC and ABAQUS, and the explicit code ABAQUS/EXPLICIT.
The imperfections measured on the real specimens before the buckling tests are introduced into the finite element model as a perturbation of the perfect cylinders surface.
The experimental imperfection measurements are unfortunately limited to the central part of the cylinders surface and the covered area has an axial length of 450 *mm*. In the finite element models, in the zones above and below this central part, the perturbation of the perfect cylinder is assumed to be a linear variation from the imperfections measured at the edge of this central part to zero imperfections in correspondence to the upper and lower ends of the cylinder.
The values of the buckling loads obtained with the three different finite element codes are in agreement.

Because of great instabilities in the numerical solution, the two implicit codes MARC and ABAQUS are not able to completely follow the post-buckling region of the curve of the axial reaction force versus the imposed displacement. The simulation analysis stops shortly after the maximum, which defines the buckling load.
However, the explicit code ABAQUS/EXPLICIT is able to follow the same curve in the post-buckling region successfully. The numerical analysis is used to simulate the experimental tests under the assumption that they are dynamic slow compression tests with an imposed displacement.
The first results obtained from a simulation on a cylinder with the [0°/45°/-45°/0°] lay-up orientation are reported here.
In Figure 18, the curve of the axial reaction force versus the imposed displacement is shown together with the measured experimental test. Two different simulations have been carried out: the first one using a mesh equal in resolution to those considered previously (length 560 *mm*, 110x28 elements), another one using a shorter model (length 520 *mm*, 110x26 elements). In the last case, where the model's length is equal to the cylinder's length without the reinforced ends, the rigidity is practically identical to the measured one.

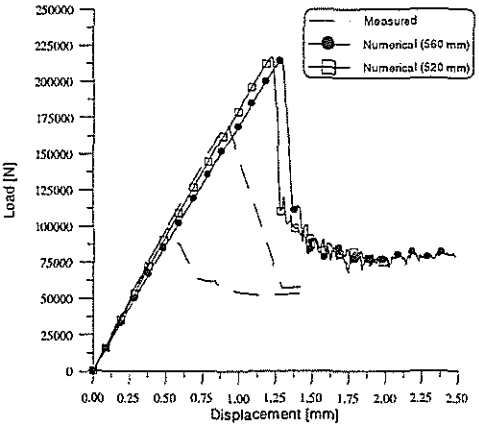

Figure 18 - Experimental-numerical comparison: different model lengths

The curves here indicate the same behaviour, but the numerical buckling load is higher than the experimentally measured. An improved value is obtained with a finer mesh (220x52 elements), as reported in Figure 19.

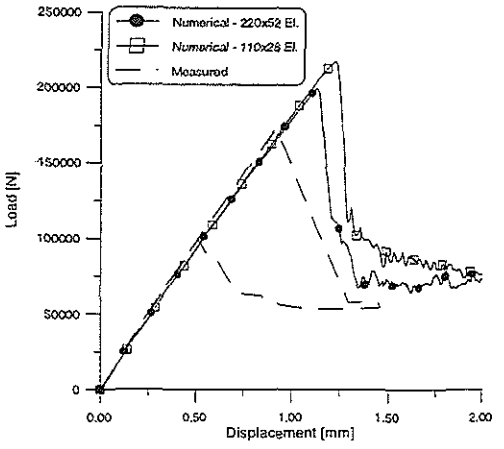

Figure 19 - Experimental-numerical comparison: different mesh resolutions

Figure 20 shows the comparison between the measured post-buckling pattern and the numerical one, obtained using a 220x52 elements mesh.
The numerical pattern contains 9 circumferential waves and 2 axial waves like those observed during the experimental test.

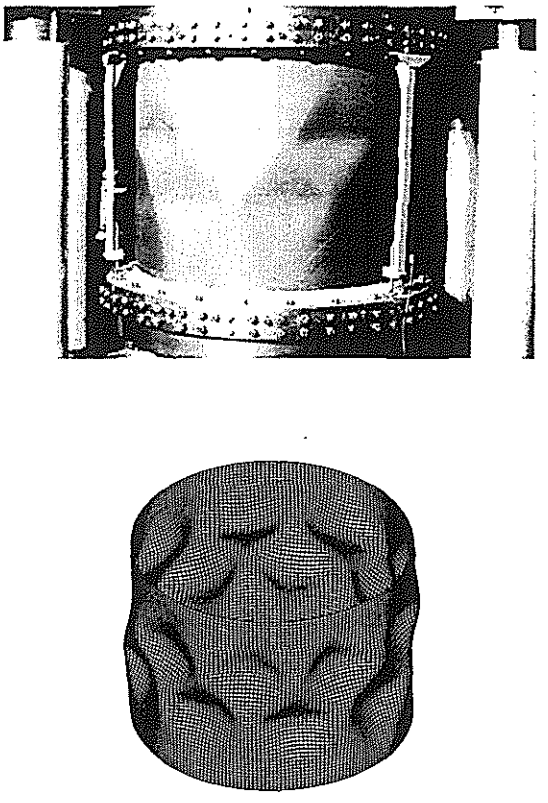

Figure 20 - Simulation with ABAQUS/EXPLICIT of the experimental test: cylinder [0°/45°/-45°/0°]

Sensitivity analysis

Using the model obtained thus far, an analysis based on different parameters has been performed to begin to understand which of these parameters mainly influences the buckling load.
This analysis is performed using the code ABAQUS/EXPLICIT and a mesh of 110x26 elements.
The results of the study on the influence of the thickness and of the layers position are presented here.
Figure 21 shows the results of the simulations obtained with the original model and with a model where the thickness has been decreased by 10%.
Figure 22 shows the results of the simulations obtained with the original model and two modified models in which the orientations of the layers at 45° are changed to 40° and 50°.

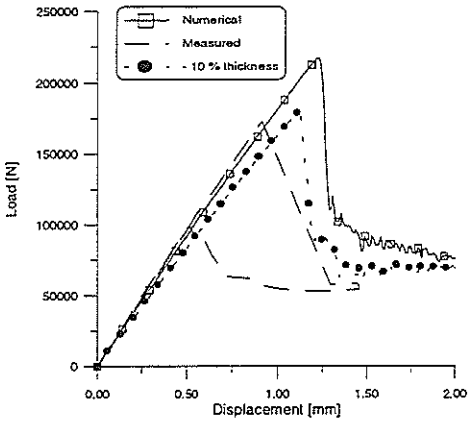

Figure 21 - Effect of the thickness variation

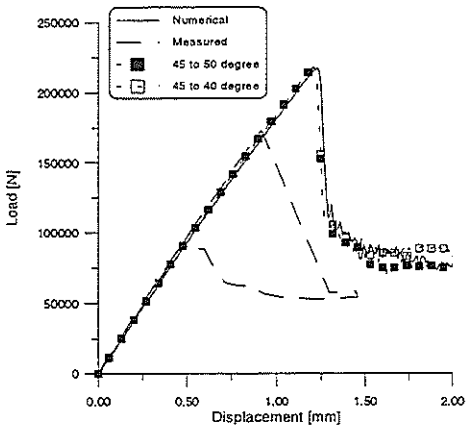

Figure 22 - Effect of the layer's position

While small variations are obtained for different layer's orientation, significant differences in the model's rigidity and in the buckling load's value are obtained for thickness variation.

Conclusions

The results of an experimental and numerical study of the buckling behaviour of carbon-epoxy laminated cylindrical shells have been presented.
Experimental buckling tests have been performed under axial compression, by a loading rig controlled in displacement. An ad-hoc equipment has allowed to measure the initial geometric imperfections and the buckling pattern development on the specimens internal surface.
The phenomena has been numerically studied by three finite element codes: MARC, ABAQUS and ABAQUS/EXPLICIT.
The finite element analysis of the cylinders without imperfections shows a great influence of the mesh accuracy on the buckling loads, even if different depending on the considered lamination. The numerical values of the buckling loads obtained by the standard eigenvalue analysis and by the non linear Riks method, using both MARC and ABAQUS implicit codes, appear in a good agreement to the analytical values, even if the convergence to those values seems quicker for ABAQUS than for MARC. On the other hand the two considered implicit codes are not able to follow the load displacement curve in the post-buckling region, due to a great instability of the solution close to the buckling load.
The influence of axisymmetric imperfections have been investigated here with MARC and ABAQUS/EXPLICIT. The obtained results, similar to ones previously obtained by the same author (Ref. 9) in the case of kevlar cylinders, show a decreasing of the buckling loads with the increasing of the imperfection's amplitude, with a higher decreasing rate for small amplitude imperfections.
The first results of a numerical simulation of a typical experimental buckling test obtained with the ABAQUS/EXPLICIT code have been presented here. The numerical buckling pattern well reproduces the measured one, while the load-displacement curves reproduce the trend of the measured ones, even if the difference between the numerical buckling load and the measured one does not appear negligible.
To well identify the reason of these differences a sensitivity analysis has been carried out, using the thickness and the layers orientation as parameters.
This model, validated also by other experimental tests, will allow to perform a wider study on the effect of the geometric imperfections and of the other parameters that mainly influence the buckling behaviour.

References

1. Hiddleton D.H., *The first fifty years of composite materials in aircraft construction*, Aeronautical Journal, vol. 96, 1992

2. Koiter W.T., *On the stability of elastic equilibrium*, Doctoral Thesis, Delft, The Netherlands, 1945, English translation: AFFDL-TR-70 25, 1970

3. Juillien J. F. et al., *Buckling of shell structures on land, in the sea and in the air*, Lyon Symposium, Elsevier Applied Science, 1991

4. Elishakoff I., Arbocz J., *Reliability of axially compressed cylindrical shells with general non symmetric imperfections*, Journal of Appl. Mech., vol. 52, March 1985

5. Simitses G.J., Shaw D., Sheinman I., *Stability of imperfect laminated cylinders: a comparison between theory and experiments*, AIAA Journal, vol. 23, n° 7, 1985

6. Giavotto V., Poggi C., Chryssanthopoulos M., *Buckling of imperfect composite shells under compression and torsion*, Proc. of Int. Meeting on Rotorcraft Basic Research, Atlanta, 1991

7. Spencer H.H., *Are measurements of geometric imperfections of plates and shells useful?*, Experimental Mechanics, vol. 18, n° 3, 1978

8. Arbocz J., Hol J.M.A.M., *The role of experiments in improving the computational models for composite shells*, Proc. of winter annual meting of American Society of Mechanical Engineers on Analitical and Computational Models of Shells, San Francisco, 1989

9. Bisagni C., *Buckling of composite shells with geometric imperfections*, Proc. of 22nd European Rotorcraft Forum, Brighton U.K., 1996

10. Bisagni C., *Buckling and post-buckling behaviour of composite cylindrical shells*, Proc. of XX ICAS Congress, Sorrento Italy, 1996

11. Bathe K. J., *Finite element procedures in engineering analysis*, Prentice-Hall, 1982

12. Riks E., *An incremental approach to the solution of snapping and buckling problems*, International Journal Solids Structures, vol. 15, 1979

13. Bisagni C., *Instabilità e comportamento post-critico di gusci in materiale composito*, Ph.D. thesis, Dipartimento di Ingegneria Aerospaziale, Politecnico di Milano, 1997